

Contents

1	Introduction	1
2	Fractional Brownian motion	2
2.1	Simulation of fractional Brownian motion	2
3	Roughness of a path	5
3.1	Estimating the roughness from discrete observations	6
3.2	Behaviour of the roughness estimator based on simulations . . .	7
4	Instantaneous volatility and realized volatility	11
4.1	Smoothness of a path by logarithmic regression	14

1 Introduction

When modelling prices of financial assets, modelling the volatility process itself plays a crucial role. In the derivatives world, log-prices are often modelled as continuous semi-martingales. For a given asset with log-price Y_t , such a process takes the form

$$dY_t = \mu_t dt + \sigma_t dW_t \quad (1)$$

where μ_t is a drift term and W_t is a one-dimensional Brownian motion. The term σ_t represents the volatility process, and it is a very important ingredient in the model (vol is rough). However, modelling the volatility process itself is also a complex task. Different approaches to estimate σ_t is used in the literature. In the simplest models, the volatility is either constant or a deterministic function of time. In more popular stochastic volatility models, the volatility process is modelled as a stochastic process itself. In notable models such as the Hull and White model, the Heston model, and the SABR model, the volatility σ_t is modelled as a continuous Brownian semi-martingale (vol is rough). The stochastic volatility models seem way more realistic but generated prices from these models are in many cases not consistent with observed prices. (33, 46)

Various authors have proposed other kinds of models to model the volatility. A popular one is stochastic volatility models driven by fractional Brownian motion. A well-known example of such a fractional stochastic volatility model is the one proposed by Comte and Renault (1998) who models the dynamics of the volatility σ_t of an asset as:

$$Y_t = \ln \sigma_t, \quad dY_t = -\gamma Y_t dt + \theta dB_t^H \quad (2)$$

where B^H is a fractional Brownian motion with Hurst exponent H . The model was first introduced to model long range dependence effect observed in financial time series. The long range dependence is modelled by choosing $1 > H > \frac{1}{2}$ (comte and renaud 1998). In recent literature starting with (vol is rough), it has been suggested to use the fractional stochastic volatility models with $H < \frac{1}{2}$ for modelling volatility. Processes driven by a fractional Brownian motion with $H < \frac{1}{2}$ are referred to as 'rough processes' since these fractional Brownian motion have trajectories rougher than a standard Brownian motion (rough vol), and (vol is rough) concludes that volatility is rough. It is important to note that (vol is rough) unlike previous literature rely on the behaviour of volatility estimators over short intraday time scales in order to asses the 'roughness'.

(rough vol) challenges the conclusions of (vol is rough). (rough vol) simulates from models where the true spot volatility is known and shows that measures of roughness for realized volatility based on the data from these simulations are in many cases much rougher than those of the underlying true spot volatility. This difference solely lies in the estimation error, and challenges the use of high-frequency volatility estimators when measuring the roughness.

In this thesis, we will take a similar approach to (rough vol) and investigate further if volatility appears to be rough even when the true model does not exhibit rough behaviour.

2 Fractional Brownian motion

A fractional Brownian motion (fBm) $(B_t^H)_{t \in \mathbb{R}}$ with Hurst parameter $H \in (0, 1)$ is a centered continuous Gaussian process with covariance function

$$\mathbb{E}[B_t^H B_s^H] = \frac{1}{2} (t^{2H} + s^{2H} - |t - s|^{2H}) \quad (3)$$

for $s, t \geq 0$. Note that B_t^H reduces to an ordinary Brownian motion for $H = \frac{1}{2}$ (specsim). The incremental process of a fractional Brownian motion is called fractional Gaussian noise, and it is a stationary discrete-time process. We define the fractional Gaussian noise $X = \{X_k : k = 0, 1, \dots\}$ by

$$X_k := B_{t_{k+1}}^H - B_{t_k}^H. \quad (4)$$

With this definition, we immediately see that every X_k is normally distribution with mean 0 and variance

$$\begin{aligned} \mathbb{E}[(B_{t_{k+1}}^H - B_{t_k}^H)^2] &= \text{Var}(B_{t_{k+1}}^H) + \text{Var}(B_{t_k}^H) - 2\text{Cov}(B_{t_{k+1}}^H, B_{t_k}^H) \\ &= t_{k+1}^{2H} + t_k^{2H} - (t_{k+1}^{2H} + t_k^{2H} - (t_{k+1} - t_k)^{2H}) = (t_{k+1} - t_k)^{2H} \end{aligned}$$

using the covariance function (3). Thus, the fractional Gaussian noise is standard normal distributed when the time step is 1.

2.1 Simulation of fractional Brownian motion

Throughout this thesis we will be simulating from the fractional Brownian motion by using a spectral method which can be used for stationary processes. The idea is to analyse the stochastic process in the spectral domain rather than the time domain. The spectral density is computed as follows for frequencies $-\pi \leq \lambda \leq \pi$:

$$f(\lambda) := \sum_{j=-\infty}^{\infty} \gamma(j) \exp(ij\lambda) \quad (5)$$

where $\gamma(\cdot)$ represent the autocovariance function. It can be shown that the spectral density of fractional Gaussian noise is given by

$$f(\lambda) = 2 \sin(\pi H) \Gamma(2H + 1) (1 - \cos \lambda) [|\lambda|^{-2H-1} + B(\lambda, H)] \quad (6)$$

where $\Gamma(\cdot)$ denotes the Gamma function and

$$B(\lambda, H) := \sum_{j=1}^{\infty} ((2\pi j + \lambda)^{-2H-1} + (2\pi j - \lambda)^{-2H-1}) \quad (7)$$

for $-\pi \leq \lambda \leq \pi$. The infinite sum makes direct numerical evaluation almost impossible. However, a useful approximation of the sum is made by (Paxson 12). They show that by using

$$\tilde{B}_3(\lambda, H) := \sum_{j=1}^3 \left((a_j^+)^{-2H-1} + (a_j^-)^{-2H-1} \right) + \frac{(a_3^+)^{-2H} + (a_3^-)^{-2H} + (a_4^+)^{-2H} + (a_4^-)^{-2H}}{8H\pi}$$

where $a_j^\pm = 2\pi j \pm \lambda$, $f(\lambda)$ is approximated quite well.

Now, consider a stationary Gaussian discrete-time process $X = \{X_n : n = 0, \dots, N-1\}$ where N is the required sample size. The spectral theorem states that it can be represented in terms of the spectral density as

$$X_n \stackrel{d}{=} \int_0^\pi \sqrt{\frac{f(\lambda)}{\pi}} \cos(n\lambda) dB_1(\lambda) - \int_0^\pi \sqrt{\frac{f(\lambda)}{\pi}} \sin(n\lambda) dB_2(\lambda) \quad (8)$$

where B_1 and B_2 are two mutually independent Brownian motions (speccsim). We wish to approximate (8). The integrand is replaced by a simpler function. Fix some integer l and set $t_k = \pi k/l$ for $k = 0, \dots, l$. Now, define a simple function $\xi_n^{(l)}$ on $[0, \pi]$ for $0 \leq n \leq N-1$ by

$$\xi_n^{(l)}(\lambda) = \sqrt{\frac{f(t_1)}{\pi}} \cos(nt_1) \mathbf{1}_{\{0\}}(\lambda) + \sum_{k=0}^{l-1} \sqrt{\frac{f(t_{k+1})}{\pi}} \cos(nt_{k+1}) \mathbf{1}_{(t_k, t_{k+1}]}(\lambda). \quad (9)$$

The first integral in (8) can be approximated by $\int_0^\pi \xi_n^{(l)}(\lambda) dB_1(\lambda)$. Since $\xi_n^{(l)}$ is a simple function the stochastic integral can be computed as

$$\int_0^\pi \xi_n^{(l)}(\lambda) dB_1(\lambda) = \sum_{j=0}^{l-1} \xi_n^{(l)}(B(t_{j+1}) - B(t_j)). \quad (10)$$

Thus, we obtain

$$\begin{aligned} \int_0^\pi \xi_n^{(l)}(\lambda) dB_1(\lambda) &= \sum_{j=0}^{l-1} \sum_{k=0}^{l-1} \sqrt{\frac{f(t_{k+1})}{\pi}} \cos(nt_{k+1}) \mathbf{1}_{(t_k, t_{k+1}]}(B_1(t_{j+1}) - B_1(t_j)) \\ &= \sum_{k=0}^{l-1} \sqrt{\frac{f(t_{k+1})}{\pi}} \cos(nt_{k+1}) (B_1(t_{k+1}) - B_1(t_k)) \\ &= \sum_{k=0}^{l-1} \sqrt{\frac{f(t_{k+1})}{\pi}} \cos(nt_{k+1}) U_k^{(0)} \sqrt{\frac{\pi}{l}} = \sum_{k=0}^{l-1} \sqrt{\frac{f(t_{k+1})}{\ell}} \cos(nt_{k+1}) U_k^{(0)} \end{aligned}$$

where $U_k^{(0)}$ is an i.i.d. standard normal random variable for $k = 0, \dots, l-1$. The $U_k^{(0)} \sqrt{\pi/\ell}$ represent the Brownian motion increments which per definition are

normally distributed with mean 0 and variance $t_{k+1} - t_k$.

The second integral in (8) can be approximated in a similar way by replacing the cosine terms with sine terms. Thus, we obtain the following approximation of X_n :

$$\hat{X}_n^{(\ell)} := \sum_{k=0}^{\ell-1} \sqrt{\frac{f(t_{k+1})}{\ell}} \left(\cos(nt_{k+1})U_k^{(0)} - \sin(nt_{k+1})U_k^{(1)} \right). \quad (11)$$

The two vectors $U^{(0)}$ and $U^{(1)}$ are mutually independent since B_1 and B_2 are independent as well. In order to calculate $\hat{X}_n^{(\ell)}$ efficiently we will be using the fast Fourier transform (FFT). To this end, we define the sequence $(a_k)_{k=0, \dots, 2\ell-1}$ by

$$a_k := \begin{cases} 0 & k = 0; \\ \frac{1}{2} \left(U_{k-1}^{(0)} + iU_{k-1}^{(1)} \right) \sqrt{\frac{f(t_k)}{\ell}} & k = 1, \dots, \ell - 1; \\ U_{k-1}^{(0)} \sqrt{\frac{f(t_k)}{\ell}} & k = \ell; \\ \frac{1}{2} \left(U_{2\ell-k-1}^{(0)} - iU_{2\ell-k-1}^{(1)} \right) \sqrt{\frac{f(t_{2\ell-k})}{\ell}} & k = \ell + 1, \dots, 2\ell - 1. \end{cases}$$

It is shown in appendix that the Fourier transform of a_k is indeed real and equals $\hat{X}_n^{(\ell)}$. From this approximated fractional Gaussian noise we can generate the fBm.

(Specsim) shows that the finite-dimensional distributions of $\hat{X}^{(\ell)}$ converge in probability to the corresponding finite-dimensional distributions of X as $\ell \rightarrow \infty$. The rate of convergence is, however, quite slow. Therefore, we will be using a $\ell \geq 30000$ when simulating from the fBm by the spectral method in this thesis in order to make sure that our simulations are reliable. Figure 1 shows three simulations of fractional Brownian motions with different Hurst parameters generated by the spectral method.

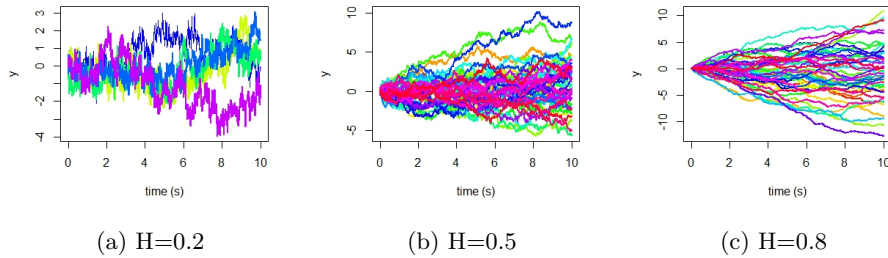


Figure 1: Fractional Brownian motions generated by the spectral method.

3 Roughness of a path

Determining the roughness of realized volatility plays a crucial role in order to make proper model specification and design estimators. We will be working with high frequency data. We observe only a single price path, and we need to measure the roughness of this path. We will closely follow the roughness indexes described in (roughvol) and (vol is rough).

We will be working with partitions of our time interval. Consider a sequence of partitions $\pi = (\pi^n)_{n \geq 1}$ of $[0, T]$ where

$$\pi^n = \left(0 = t_0^n < t_1^n < \dots < t_{N(\pi^n)}^n = T\right)$$

represents observation times at frequency n . Here $N(\pi^n)$ denotes the number of intervals in the partition π^n . For the time partitions we will be working with in this thesis we will assume that

$$|\pi^n| := \sup_{i=1, \dots, N(\pi^n)} |t_i^n - t_{i-1}^n| \xrightarrow{n \rightarrow \infty} 0. \quad (12)$$

That is, the size of the largest interval of π^n will converge to 0 as $n \rightarrow \infty$.

We will now define the concept of p -th variation along a sequence of partitions $(\pi^n)_{n \geq 1}$. The definition follows the definition from (Cont and Perkowski 2019).

Definition 1. (*p -th variation along a sequence of partitions*) $x \in C^0([0, T], \mathbb{R})$ has finite p -th variation along the sequence of partitions $\pi = (\pi^n, n \geq 1)$ if there exists a continuous increasing function $[x]_\pi^{(p)} : [0, T] \rightarrow \mathbb{R}_+$ such that

$$\forall t \in [0, T], \quad \sum_{\{t_j^n, t_{j+1}^n\} \in \pi^n : t_j^n \leq t} |x(t_{j+1}^n) - x(t_j^n)|^p \xrightarrow{n \rightarrow \infty} [x]_\pi^{(p)}(t). \quad (3)$$

If this property holds, then the convergence in (3) is uniform. We call $[x]_\pi^{(p)}$ the p -th variation of x along the sequence of partitions π . We denote $V_\pi^p([0, T], \mathbb{R})$ the set of all continuous paths with finite p -th variation along π .

We further define the concepts of variation index and roughness index of a path following (rough vol).

Definition 2 (Variation index). The variation index of a path x along a partition sequence π is defined as the smallest $p \geq 1$ for which x has finite p -th variation along π :

$$p^\pi(x) = \inf \{p \geq 1 : x \in V_\pi^p([0, T], \mathbb{R})\}.$$

Definition 3 (Roughness index). The roughness index of a path x (along π) is

defined as

$$H^\pi(x) = \frac{1}{p^\pi(x)}.$$

When the underlying sequence of partitions is clear, we will simply denote these indexes as $p(x)$ and $H(x)$.

For a real-valued stochastic process $X : [0, T] \times \Omega \rightarrow \mathbb{R}$ the variation index (hence also the roughness index) $p^\pi(X(., \omega))$ of each sample path $X(., \omega)$ may in principle be different. However, there are many important classes of stochastic processes which have an almost-sure roughness index. This holds for example for a fractional Brownian motion where the roughness index matches with the corresponding Hurst parameter (rough vol).

When estimating roughness from empirical data based on discrete observations, using the p -th variation directly is difficult since it involves checking convergence to an unknown limit. To this end, we introduce the concept of normalized p -th variation.

Definition 4 (Normalized p -th variation along a sequence of partitions). *Let π be a sequence of partitions of $[0, T]$ with mesh $|\pi^n| \rightarrow 0$ and $\pi^n = \{0 = t_1^n < t_2^n < \dots < t_{N(\pi^n)}^n = T\}$. $x \in V_\pi^p([0, T], \mathbb{R})$ is said to have normalized p -th variation along π if there exists a continuous function $w(x, p, \pi) : [0, T] \rightarrow \mathbb{R}$ such that:*

$$\forall t \in [0, T], \quad \sum_{\pi^n \cap [0, t]} |x(t_{j+1}^n) - x(t_j^n)|^p \rightarrow w(x, p, \pi)(t).$$

(Cont and Das 2022) shows that for a large class of functions with p -th variation, the normalized p -th variation exists and is linear. Furthermore, (rough vol) shows that the normalized p -th variation is a 'sharp' statistic meaning that if a function has finite p -th variation then for all $q \neq p$ the normalized p -th variation is either zero or infinite. Additionally, it is shown that a fractional Brownian motion has normalized p -th variation along the dyadic partition $\mathbb{T} = (\mathbb{T}^n)_{n \geq 1}$ almost-surely.

3.1 Estimating the roughness from discrete observations

With these concepts defined we now proceed to explaining how roughness can be estimated from discrete observations. Given discrete observations on a refining partition π^L we define the 'normalized p -th variation statistic' which is the discrete counterpart of the normalized p -th variation:

$$W(L, K, \pi, p, t, X) := \sum_{\pi^K \cap [0, t]} \frac{|X(t_{i+1}^K) - X(t_i^K)|^p}{\sum_{\pi^L \cap [t_i^K, t_{i+1}^K]} |X(t_{j+1}^L) - X(t_j^L)|^p} \times (t_{i+1}^K - t_i^K). \quad (13)$$

This definition involves two frequencies K and $L \gg K$. We can consider L as the sample frequency while K is a block frequency such that π^K is a subpartition of π^L . Thus, we are grouping the sample size L into K many groups where each group contains exactly $\frac{L}{K}$ consecutive points. It can be seen that the normalized p -th variation statistic converges to the normalized p -th variation as L and K increase. That is,

$$\lim_{K \rightarrow \infty} \lim_{L \rightarrow \infty} W(L, K, \pi, p, t, X) = w(x, p, \pi)(t). \quad (14)$$

The variation index estimator $\hat{p}_{L,K}^\pi(X)$ associated with data sampled on π^L can then be obtained by computing $W(L, K, \pi, p, t, X)$ for different values of p such that the following equation can be solved for $\hat{p}_{L,K}^\pi(X)$

$$W(L, K, \pi, \hat{p}_{L,K}^\pi(X), t, X) = T. \quad (15)$$

The corresponding roughness index estimator is then defined as

$$\hat{H}_{L,K}^\pi(X) = \frac{1}{\hat{p}_{L,K}^\pi(X)}.$$

If the underlying dataset and partition is clear we will also denote these estimators as $\hat{p}_{L,K}$ and $\hat{H}_{L,K}$. Asymptotic properties of these estimators under high-frequency sampling are studied in (comte and das 2022).

3.2 Behaviour of the roughness estimator based on simulations

We will now study the behaviour of the roughness estimator based on high-frequency simulated data. We will be simulating from a fractional Brownian motion and compute the roughness estimator based on the data. In this simulation section we will be using a uniform partition of the time interval $[0, 1]$ with

$$\pi^n = \left(0 < \frac{1}{n} < \frac{2}{n} < \dots < 1 \right).$$

We will be simulating from four fractional Brownian motions with four different Hurst exponents $H = \{0.1, 0.3, 0.5, 0.8\}$ in order to investigate the accuracy of the roughness estimator $\hat{H}_{L,K}^\pi(X)$. First, we plot $\log(W(L = 300 \times 300, K = 300, \pi, p, t = 1, X = B^H))$ against $H = 1/p$ to visualize the estimation. The results are presented in Figure 2. The solid black line is the value of $\log(W(L = 300 \times 300, K = 300, \pi, p, t = 1, X = B^H))$ for different values of $1/p$. The blue vertical line represents the estimated roughness index whereas the black dotted vertical line represent the true Hurst parameter. The blue horizontal line represents $W(L, K, \pi, p, t, X) = T$. The estimated roughness index $\hat{H}_{L,K}^\pi$ is the crossing between $\log(W(L = 300 \times 300, K = 300, \pi, p, t = 1, X = B^H))$ and $W(L, K, \pi, p, t, X) = T$.

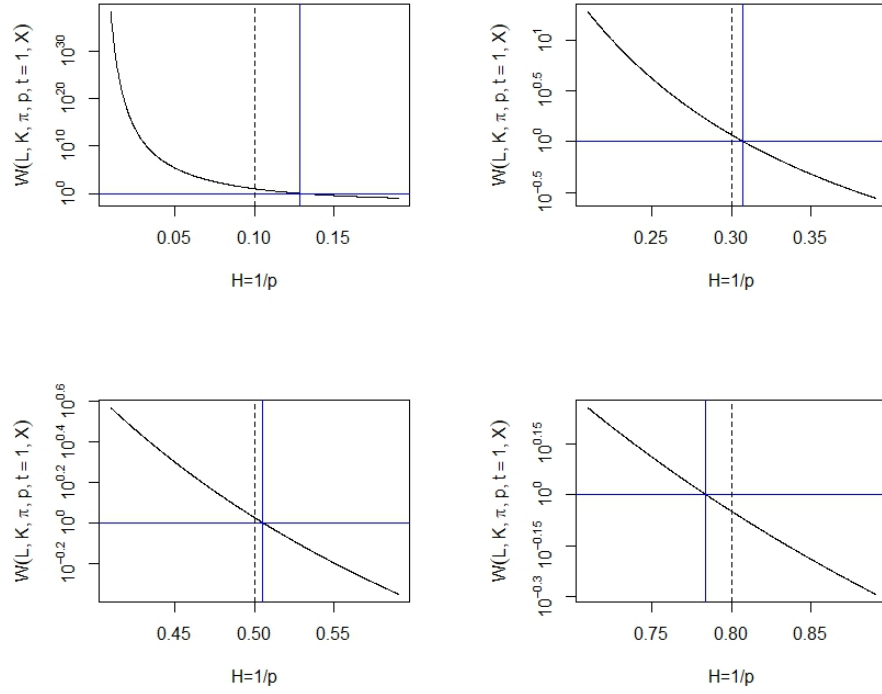


Figure 2: Log-scale plot of the normalized p -th variation statistic for fBm with Hurst parameter $H = \{0.1, 0.3, 0.5, 0.8\}$. The black solid line represents the value of $\log(W(L = 300 \times 300, K = 300, \pi, p, t = 1, X = B^H))$ plotted against $H = 1/p$. The blue vertical line represents $\hat{H}_{L,K}$ using the normalized p -th variation statistic with $L = 300 \times 300$ and $K = 300$. The vertical black dotted line represents the true Hurst parameter.

In Figure 3, we have created histograms of the estimator $\hat{H}_{L,K}$ again by using $W(L = 300 \times 300, K = 300, \pi, p, t = 1, X = B^H)$ from 150 independent simulations. In addition to this, Table 1 provides the summary statistics for the estimated roughness index $\hat{H}_{L,K}$ shown in the histograms. Based on Figure 2 and 3, and Table 1, we conclude that the estimated roughness index $\hat{H}_{L,K}$ seems to be fairly accurate when used on a data set with length $L = 300 \times 300$ generated from a fractional Brownian motion. All the estimated $\hat{H}_{L,K}$ are within a distance 0.05 from the true Hurst parameter, and the mean and median of the estimated roughness are in all cases very close to the true Hurst parameter indicating that our estimator is quite accurate. Only exception is for the fBm with Hurst parameter $H = 0.8$ where even the upper quartile of $\hat{H}_{L,K}$ is smaller than the true Hurst parameter as seen in Table 1. This suggest that the estimated roughness index might be biased downwards in the case of $H = 0.8$. The estimate is, however, still quite accurate even for $H = 0.8$.

H	Min.	Lower quartile	Median	Mean	Upper quartile	Max.
0.1	0.0622	0.0944	0.1021	0.1031	0.1149	0.1402
0.3	0.2746	0.2954	0.3012	0.3005	0.3052	0.3177
0.5	0.4743	0.4954	0.5004	0.4997	0.5041	0.5239
0.8	0.7657	0.7797	0.7856	0.7865	0.7937	0.8239

Table 1: Summary of statistics for estimated roughness index $\hat{H}_{L,K}$ from 150 independent simulations of fBm with $L = 300 \times 300$ and $K = 300$.

In Figure 4 we have used $L = 2000 \times 2000$ and $K = 2000$ to make similar plots to those in Figure 2 and Figure 3 for a fractional Brownian motion with Hurst parameter $H = 0.1$. Table 2 provides the summary statistics for the estimated roughness index $\hat{H}_{L,K}$ corresponding to the histogram in Figure 4. We observe that the results are similar to those we obtained for $L = 300 \times 300$ and $K = 300$ but that the estimated roughness index $\hat{H}_{L,K}$ seems to be even more accurate as seen in Figure 4 and Table 2. This is not surprising since we know that the normalized p -th variation statistic converges to the normalized p -th variation as L and K increase. However, increasing L and K is also computationally more demanding. The accuracy of $\hat{H}_{L,K}$ when using $L = 300 \times 300$ and $K = 300$ is satisfactory for many of our purposes. Therefore, we will be using at least $L = 300 \times 300$ and $K = 300$ for the remainder of the thesis.

H	Min.	Lower quartile	Median	Mean	Upper quartile	Max.
0.1	0.0892	0.0963	0.0996	0.0998	0.1031	0.1145

Table 2: Summary of statistics for estimated roughness index $\hat{H}_{L,K}$ from 150 independent simulations of fBm with $H = 0.1$, $L = 2000 \times 2000$ and $K = 2000$.

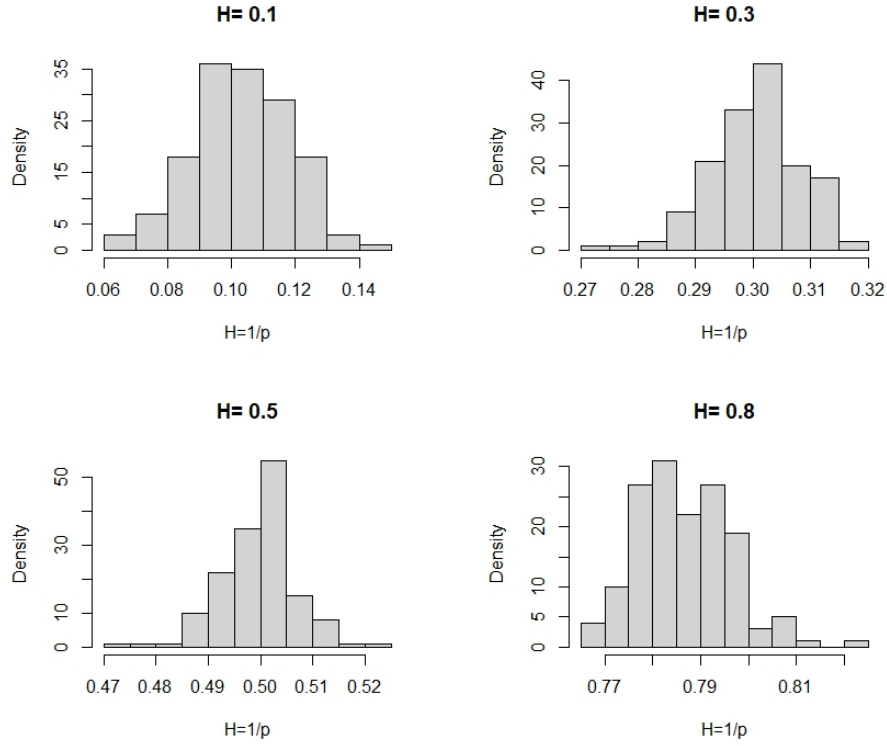


Figure 3: Histogram of estimated roughness index $\hat{H}_{L,K}$ with $L = 300 \times 300$ and $K = 300$ generated from 150 independent simulation of fractional Brownian motions with Hurst parameter $H = \{0.1, 0.3, 0.5, 0.8\}$.

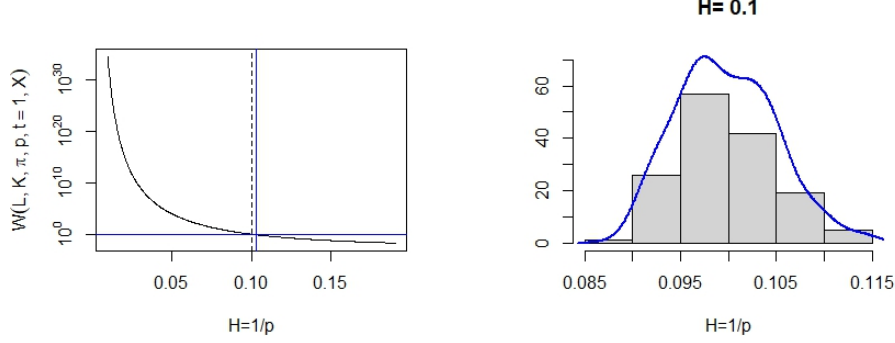


Figure 4: Simulation results for fractional Brownian motion with Hurst parameter $H = 0.1$. **Left:** The value of $\log(W(L = 2000 \times 2000, K = 2000, \pi, p, t = 1, X = B^H))$ plotted against $H = 1/p$ in black. The blue vertical line represents the estimated roughness $\hat{H}_{L,K}$ using $L = 2000 \times 2000$ and $K = 2000$. The vertical black dotted line represents the true Hurst parameter. **Right:** Histogram of estimated roughness index $\hat{H}_{L,K}$ using $L = 2000 \times 2000$ and $K = 2000$ generated by 150 independent simulations of fBm with Hurst parameter $H = 0.1$. The blue line represents a kernel estimator for density.

We further investigate how the choice of $K \ll L$ affects the estimated roughness index $\hat{H}_{L,K}$. In Figure 5, we have plotted the estimated roughness $\hat{H}_{300 \times 300, K}$ for a fractional Brownian motion with Hurst parameter $H = 0.1$ for different values of K with a fixed $L = 300 \times 300$. Note that when $\frac{L}{K}$ is not an integer, the K many groups from the definition of normalized p -th variation statistic (13) do not contain exactly $\frac{L}{K}$ consecutive points. The code is implemented such that each group will contain either $\lceil \frac{L}{K} \rceil$ or $\lfloor \frac{L}{K} \rfloor$ consecutive points. Figure 5 shows that when K is too low, the estimator $\hat{H}_{300 \times 300, K}$ seems to be underestimating the true Hurst parameter whereas when K is too high the Hurst parameter is overestimated. For $K \approx \sqrt{L}$ the estimated roughness index is quite consistent and close to the true Hurst parameter $H = 0.1$. It is thus natural to use $K = \sqrt{L}$ since $\frac{L}{K}$ will be an integer and the estimator $\hat{H}_{L,K}$ seems to be accurate and consistent in that range.

3.3 Instantaneous volatility and realized volatility

As mentioned in (1) log-prices are often modelled as continuous semi-martingales where the derivative of the log-price Y_t takes the form

$$dY_t = \mu_t dt + \sigma_t dW_t.$$

The term σ_t represents the volatility process, and σ_t is also called instantaneous volatility or spot volatility. In stochastic volatility models, σ_t is represented as a

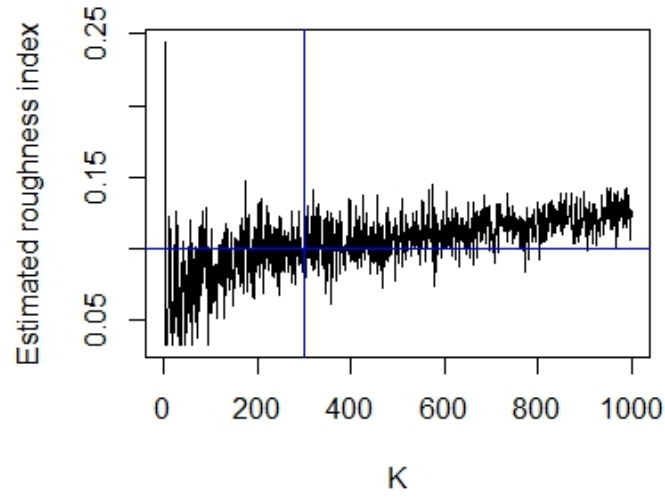


Figure 5: The solid black line represents the estimated roughness index $\hat{H}_{300 \times 300, K}$ plotted against different values of K for a simulation from a fBm with Hurst parameter $H = 0.1$. The blue vertical line represents $K = \sqrt{L} = 300$ whereas the blue horizontal line represents the true Hurst parameter $H = 0.1$.

stochastic process itself often driven by a fractional process. Contrary to prices of an asset, instantaneous volatility cannot be directly observed and needs to be estimated from prices.

In a practical situation, the price of the asset S_t at time t is usually observed over a non-uniform time grid of $[0, T]$:

$$\pi^n = \left(0 = t_0^n < t_1^n < \dots < t_{N(\pi^n)}^n = T\right).$$

For high-frequency data the assumption (12) is often assumed. That is, $|\pi^n| \rightarrow 0$ as n increases where n can be thought of as a sampling frequency i.e. the number of samples per second (or per other unit).

For $Y_t = \log(S_t)$ the instantaneous volatility σ_t can be recovered (use Itô from FinCont!!) by

$$\sigma_t^2 = \frac{d}{dt} \lim_{n \rightarrow \infty} \sum_{\pi^n \cap [0, t]} (Y(t_{i+1}^n) - Y(t_i^n))^2 = \lim_{n \rightarrow \infty} RV_t^2(\pi^n)^2$$

where the realized variance along the sampling grid π^n is defined as

$$RV_t^2(\pi^n)^2 = \sum_{\pi^n \cap [0, t]} (Y(t_{i+1}^n) - Y(t_i^n))^2.$$

The realized volatility over time interval $[t, t + \Delta]$ along the sampling grid π^n is then defined as

$$RV_{t, t+\Delta}(\pi^n) = \sqrt{\sum_{\pi^n \cap [t, t+\Delta]} (Y(t_{i+1}^n) - Y(t_i^n))^2}. \quad (16)$$

If the price S_t follows a stochastic volatility model as, it is known that the realized variance converges to the quadratic variation of Y as sampling frequency increases (Jacod and Protter)

$$RV_{t, t+\Delta}(\pi^n) \xrightarrow[n \rightarrow \infty]{\mathbb{P}} \sqrt{\int_t^{t+\Delta} \sigma_u^2 du}.$$

Hence, along a single price path observed at high-frequency, we can compute the realized volatility (16) and use this as an indicator of volatility

$$RV_{t, t+\Delta}(\pi^n) \simeq \sqrt{\Delta} \sigma_t.$$

As n increases the estimation becomes more accurate (roughvol).

3.4 Smoothness of a path by logarithmic regression

Consider a volatility process on a time grid $[0, T]$. If we pretend that we have access to discrete observations of the spot volatility process with mesh Δ such

that the observations are $\sigma_0, \sigma_\Delta, \dots, \sigma_{k\Delta}, \dots$ for $k \in \{0, \lfloor T/\Delta \rfloor\}$. Here Δ is a natural number and $\Delta \geq 1$. If we set $N = \lfloor T/\Delta \rfloor$, then for $q \geq 0$ we define

$$m(q, \Delta) = \frac{1}{N} \sum_{k=1}^N |\log(\sigma_{k\Delta}) - \log(\sigma_{(k-1)\Delta})|^q.$$

Following (vol is rough) the main assumption is that for some $s_q > 0$ and $b_q > 0$

$$N^{qs_q} m(q, \Delta) \rightarrow b_q \quad (17)$$

as Δ tends to zero. Under additional technical assumptions, this essentially means that the volatility process belongs to a Besov smoothness space $\mathcal{B}_{q,\infty}^{s_q}$ and does not belong to $\mathcal{B}_{q,\infty}^{s'_q}$ for $s'_q > s_q$. Hence, s_q can be considered as a smoothness parameter. In particular, if $\log(\sigma_t)$ is a fractional Brownian motion with Hurts parameter H , then for any $q \geq 0$ equation (17) holds in probability with $s_q = H$. It can further be shown that the sample paths of the process do indeed belong to $\mathcal{B}_{q,\infty}^{s_q}$. Thus, s_q is a measure of the smoothness (or roughness) of the volatility process (vol is rough).

The instantaneous volatility can not be directly observed, and exact computations of $m(q, \Delta)$ is not possible in practice. In order to make use of $m(q, \Delta)$ we must therefore approximate the true spot volatility. The estimated volatility can be computed by the realized volatility or some variation of realized volatility. In the following we will be using the notation $m(q, \Delta)$ with the understanding that we are only approximating the true spot volatility. To estimate the smoothness parameter s_q for each q , we can compute $m(q, \Delta)$ for different values of Δ and regress $\log m(q, \Delta)$ against $\log \Delta$. Note that for a given Δ several $m(q, \Delta)$ can be computed depending on the starting point. For example, if $\Delta = 3$ then the starting point can be $\hat{\sigma}_0, \hat{\sigma}_\Delta$ or $\hat{\sigma}_{2\Delta}$. The final measure of $m(q, \Delta)$ is computed as the average of these values of $m(q, \Delta)$ with different starting points.

(Vol is rough) shows that for a given q , $\log m(q, \Delta)$ values regressed against $\log \Delta$ essentially lie on a straight line. Assuming stationary increments of the log-volatility, this implies that the increments fulfil the scaling property

$$\mathbb{E} [|\log(\sigma_\Delta) - \log(\sigma_0)|^q] = b_q \Delta^{\zeta_q}$$

where $\zeta_q = qs_q > 0$ is the slope of the line associated to q . This result uses that $m(q, \Delta)$ can be seen as the empirical counterpart of $\mathbb{E} [|\log(\sigma_\Delta) - \log(\sigma_0)|^q]$. Furthermore, (vol is rough) shows that s_q seems to not depend on q , and plotting ζ_q against q shows $\zeta_q \sim qs_q$.

Thus, we can compute an estimate of the smoothness (or roughness) of a volatility process by first regressing $\log m(q, \Delta)$ against $\log \Delta$ for different values of q . The slope of the straight line is an estimate of ζ_q . Next, we regress ζ_q against q . The slope of the straight line is and estimate of the smoothness parameter

s_q . For a fractional Brownian motion $s_q = H$ where H is the Hurst parameter.

In Figure 6 we have replicated the method used in (vol is rough) to estimate the roughness index of the volatility of S&P500 using the first 3500 days of the daily realized variance estimates from the Oxford-Man Institute of Quantitative Finance Realized Library for S&P. Our results coincide with the results from (vol is rough), and the log-regression yields a straight line for all our values of q . Our estimated smoothness of the S&P500 volatility is $H = 0.1421$.

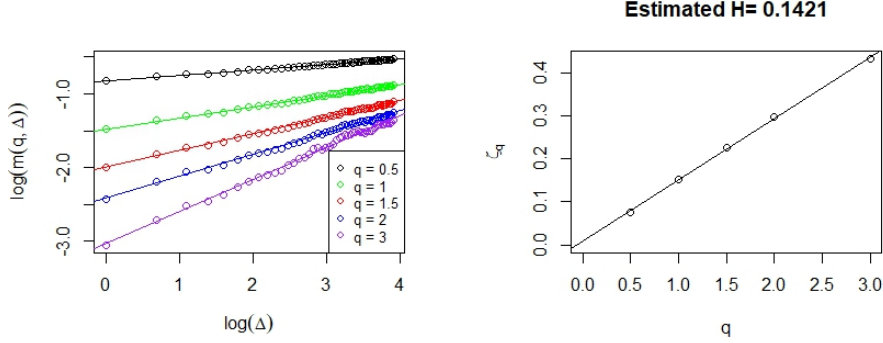


Figure 6: A reproduction of the log-regression method introduced by (vol is rough) using the first 3500 days of the daily realized variance estimates from the Oxford-Man Institute of Quantitative Finance Realized Library for S&P. The estimated roughness is $H = 0.1421$.

In Figure 7 we have used the roughness estimator from section 3.1 on the same S&P500 volatility data to estimate the roughness. We have used $W(L = 3500, K = \sqrt{3500}, \pi, p, t = 1, X)$ since the dataset only consist of 3500 days. We have set $t = 1$ since t simply works as a scaling parameter. The conclusions are the same for $t = 1$ as for $t = 3500$. The estimated roughness index is $\hat{H}_{L,K} = 0.1425$. We immediately observe that the estimated roughness index is very close to the estimated smoothness parameter from the log-regression method $s_q = 0.1421$. However, note that $L = 3500$ is much smaller than $L = 300 \times 300 = 90000$ for which we have investigated the accuracy of the roughness estimator via normalized p -th variation statistic. Therefore, the estimated roughness estimator $\hat{H}_{L,K}$ might not be very precise. The results do however indicate that our two different approaches to estimate the roughness of a volatility process coincides.

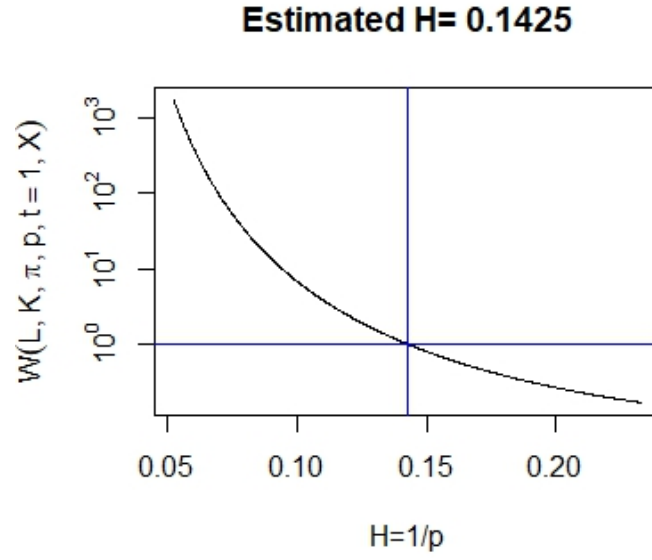


Figure 7: Estimating the roughness of the first 3500 days of S&P500 volatility data from Oxford-Man Institute of Quantitative Finance Realized Library using the roughness estimator from section 3.1 with $L = 3500$ and $K = \sqrt{3500}$. The estimated roughness index is $\hat{H}_{L,K} = 0.1425$.

A Spectral Method FFT

Consider

$$a_k := \begin{cases} 0 & k = 0; \\ \frac{1}{2} \left(U_{k-1}^{(0)} + iU_{k-1}^{(1)} \right) \sqrt{\frac{f(t_k)}{\ell}} & k = 1, \dots, \ell - 1; \\ U_{k-1}^{(0)} \sqrt{\frac{f(t_k)}{\ell}} & k = \ell; \\ \frac{1}{2} \left(U_{2\ell-k-1}^{(0)} - iU_{2\ell-k-1}^{(1)} \right) \sqrt{\frac{f(t_{2\ell-k})}{\ell}} & k = \ell + 1, \dots, 2\ell - 1. \end{cases}$$

We want to take the Fourier transform of this sequence. The Fourier transform of $(a_k)_{k=0}^{2\ell-1}$ is $\lambda_n = \sum_{k=0}^{2\ell-1} a_k \exp(2\pi i \frac{nk}{2\ell})$. By Euler's formula we obtain

$$\lambda_n = \sum_{k=0}^{2\ell-1} a_k \left(\cos\left(\pi \frac{nk}{\ell}\right) + i \sin\left(\pi \frac{nk}{\ell}\right) \right).$$

We will now insert a_k and split the sum into the four different cases of a_k . Hence, we obtain

$$\begin{aligned} \lambda_n &= 0 + \sum_{k=1}^{\ell-1} \frac{1}{2} \left(U_{k-1}^{(0)} + iU_{k-1}^{(1)} \right) \sqrt{\frac{f(t_k)}{\ell}} \left(\cos\left(\pi \frac{nk}{\ell}\right) + i \sin\left(\pi \frac{nk}{\ell}\right) \right) \\ &\quad + U_{\ell-1}^{(0)} \sqrt{\frac{f(t_\ell)}{\ell}} \left(\cos\left(\pi \frac{n\ell}{\ell}\right) + i \sin\left(\pi \frac{n\ell}{\ell}\right) \right) \\ &\quad + \sum_{k=\ell+1}^{2\ell-1} \frac{1}{2} \left(U_{2\ell-k-1}^{(0)} - iU_{2\ell-k-1}^{(1)} \right) \sqrt{\frac{f(t_{2\ell-k})}{\ell}} \left(\cos\left(\pi \frac{nk}{\ell}\right) + i \sin\left(\pi \frac{nk}{\ell}\right) \right). \end{aligned}$$

By definition $t_k = \frac{\pi k}{\ell}$. Thus, what is inside the cosine and sine functions is simply nt_k . Note that for $k = \ell$ we have $t_k = \pi$. Thus, $\sin(nt_\ell) = 0$ since n is an integer. By inserting this and changing the indexes of the two sums, we obtain

$$\begin{aligned} \lambda_n &= U_{\ell-1}^{(0)} \sqrt{\frac{f(t_\ell)}{\ell}} \cos(nt_\ell) \\ &\quad + \sum_{k=0}^{\ell-2} \frac{1}{2} \left(U_k^{(0)} + iU_k^{(1)} \right) \sqrt{\frac{f(t_{k+1})}{\ell}} (\cos(nt_{k+1}) + i \sin(nt_{k+1})) \\ &\quad + \sum_{k=0}^{\ell-2} \frac{1}{2} \left(U_{\ell-k-2}^{(0)} - iU_{\ell-k-2}^{(1)} \right) \sqrt{\frac{f(t_{\ell-k-1})}{\ell}} (\cos(nt_{\ell-k-1}) + i \sin(nt_{\ell-k-1})). \end{aligned}$$

Now note that $\sin(nt_{\ell-k-1}) = -\sin(nt_{\ell-(k+1)})$ since $t_\ell = \pi$. Similarly, $\cos(nt_{\ell-k-1}) = \cos(nt_{\ell-(k+1)})$. By inserting that in the last sum in the above expression, the

sum becomes

$$\begin{aligned}
& \sum_{k=0}^{l-2} \frac{1}{2} \left(U_{\ell-k-2}^{(0)} - iU_{\ell-k-2}^{(1)} \right) \sqrt{\frac{f(t_{\ell-k-1})}{\ell}} (\cos(nt_{\ell-k-1}) - i \sin(nt_{\ell-k-1})) \\
&= \sum_{k=0}^{l-2} \frac{1}{2} \left(U_k^{(0)} - iU_k^{(1)} \right) \sqrt{\frac{f(t_{k+1})}{\ell}} (\cos(nt_{k+1}) - i \sin(nt_{k+1}))
\end{aligned}$$

where we have reversed the sum order. Now we can combine the two sums into one. Several terms cancel out such that we obtain

$$\begin{aligned}
\lambda_n &= U_{\ell-1}^{(0)} \sqrt{\frac{f(t_\ell)}{\ell}} \cos(nt_\ell) + \sqrt{\frac{f(t_{k+1})}{\ell}} \sum_{k=0}^{l-2} \left(U_k^{(0)} \cos(nt_{k+1}) - U_k^{(1)} \sin(nt_{k+1}) \right) \\
&= \sum_{k=0}^{l-1} \sqrt{\frac{f(t_{k+1})}{\ell}} \left(U_k^{(0)} \cos(nt_{k+1}) - U_k^{(1)} \sin(nt_{k+1}) \right)
\end{aligned}$$

which equals the definition of $\hat{X}_n^{(\ell)}$ from (11) as desired.